OXFORD

Human Molecular Genetics, 2024, Vol. 33, 5, 387–399
https://doi.org/10.1093/hmg/ddad191
Advance access publication date 8 November 2023
Original Article

Age- and region-dependent cortical excitability in the zQ175 Huntington disease mouse model

Yundi Wang[1], Daniel Ramandi[1,2], Marja D. Sepers[1], James P. Mackay[1], Lynn A. Raymond[1,*]

[1]Department of Psychiatry and Djavad Mowafaghian Centre for Brain Health, 2215 Wesbrook Mall, Vancouver, V6T 1Z3, Canada
[2]Graduate Program in Cell and Developmental Biology, University of British Columbia, 2350 Health Sciences Mall, Vancouver, V6T 2A1, Canada
[*]Corresponding author. Department of Psychiatry and Djavad Mowafaghian Centre for Brain Health, 5603-2215 Wesbrook Mall, Vancouver, BC V6T 1Z3, Canada. E-mail: lynn.raymond@ubc.ca

Abstract

The neurodegenerative disorder, Huntington disease (HD), manifests as disorders of movement, cognition and mood. Although studies report abnormal corticostriatal synaptic function early in HD mouse models, less is known about cortical–cortical activity across brain regions and disease stages. Recently, we reported enhanced mesoscale spread of cortical responses to sensory stimulation *in vivo* at early-manifest stages of two HD mouse models. Here, we investigated cortical excitability of zQ175 HD-model mice compared to their wild-type littermates across different cell types, ages and/or cortical regions using *ex vivo* electrophysiology. Cortical pyramidal neurons (CPNs) in somatosensory cortex of zQ175 mice showed intrinsic hyper-excitability at 3–4 months, but hypo-excitability at early-manifest stage (8–9 months); reduced frequency of spontaneous excitatory postsynaptic currents (sEPSCs) was seen at both ages. In contrast, motor cortex CPNs in early-manifest zQ175 mice showed increased intrinsic excitability and sEPSC frequency. Large-amplitude excitatory discharges recorded from CPNs in early-manifest zQ175 mice showed increased frequency only in somatosensory cortex, suggesting the intrinsic hypo-excitability of these CPNs may be compensatory against cortical network hyper-excitability. Similarly, in early-manifest zQ175 mice, region-dependent differences were seen in fast-spiking interneurons (FSIs): somatosensory but not motor FSIs from early-manifest zQ175 mice had reduced intrinsic excitability. Moreover, CPNs showed decreased frequency of spontaneous inhibitory postsynaptic currents and increased excitatory-inhibitory (E-I) balance of evoked synaptic currents in somatosensory cortex. Aberrant large-amplitude discharges and reduced inhibitory drive may therefore underlie E-I imbalances that result in circuit changes and synaptic dysfunction in early-manifest HD.

Keywords: Huntington disease; sensorimotor; cortex; excitability; electrophysiology

Introduction

Huntington Disease (HD), an autosomal dominant neurodegenerative disorder, is caused by abnormal expansions > 39 of the CAG trinucleotide repeat in the Huntingtin gene encoding the huntingtin protein (Htt) [1]. Preceding neurodegeneration and the manifestation of movement disorders, cognitive impairment and neuropsychiatric symptoms, there are early circuit changes and synaptic dysfunction [2]. Although preliminary genetic approaches to lower Htt in the brain are under development [3], they may not fully restore circuitry and synaptic function [4], necessitating a better understanding of these cellular and synaptic mechanisms of HD in order to develop disease-modifying therapies.

In HD, a substantial body of *ex vivo* electrophysiological studies have focused on the striatum. These studies revealed changes across disease stages in spiny projection neuron (SPN) membrane properties and excitability; the activity of fast-spiking parvalbumin and persistent firing somatostatin interneurons (INs); and, modifications in synaptic input from both cortical and thalamic glutamatergic afferents [2, 5–7]. Specifically, these studies reported early increased excitatory input to SPNs followed by loss of cortical and thalamic input at later stages. Further, a prominent early change in SPNs is augmented extrasynaptic NMDA-type glutamate receptor (eNMDAR) expression and function, contributing to suppression of neuronal survival signaling and altered synaptic plasticity [8–13]. The earliest pathological changes in HD however, occur in both the striatum and cortex [14]. In patients with HD, posterior cortical regions that mediate visuo-spatial processing show early thinning on magnetic resonance imaging (MRI) [15] and by late stages of HD, cortical thickness is reduced by > 30% [16]. Moreover, studies have suggested a key role of aberrant cortical input to striatal SPNs in driving their dysfunction and eventual degeneration [17–19], highlighting the importance of examining cortical cellular mechanisms of HD.

Excitatory-inhibitory (E-I) balance in cortical circuits is critical to normal brain function [20]. Using *in vivo* cortical mesoscale imaging and multi-electrode recording, we recently demonstrated enhanced spread of cortical activity across brain regions in response to sensory stimulation, in the early-manifest stage of both YAC128 and zQ175 mouse models of HD [21]. Such altered sensory-evoked cortical activity may contribute to deficits in sensory discrimination learning and cortical plasticity after sensory deprivation reported in presymptomatic R6/1 mice [22]. Previous *ex vivo* electrophysiological studies report varying changes in excitatory vs. inhibitory input to cortical pyramidal neurons (CPNs) across disease stage and HD mouse models [21, 23–25], though none have examined sensory cortex in zQ175 mice. As well, increased large-amplitude excitatory network

Received: July 17, 2023. **Revised:** September 29, 2023. **Accepted:** November 2, 2023

Table 1. Cortical pyramidal neuron membrane properties of 3–4 and 8–9 month old zQ175 and WT mice.

		Cm (pF)	Rm (MΩ)
Sensory cortex			
3–4 months			
	zQ175 (13)	99.5 ± 9.2	142.3 ± 10.1
	WT (20)	119.9 ± 6.0	136.4 ± 7.8
8–9 months			
	zQ175 (19)	102.3 ± 4.7	156.1 ± 7.8
	WT (19)	111.9 ± 7.3	143.1 ± 8.5
	CsMe zQ175 (20)	113.8 ± 6.4	136.8 ± 9.5
	CsMe WT (21)	107.1 ± 5.7	147.2 ± 8.9
Motor cortex			
8–9 months			
	zQ175 (16)	119.5 ± 7.4	132.7 ± 9.5
	WT (14)	108.3 ± 6.7	135.9 ± 8.6

Unless otherwise indicated, all measurements were acquired using a K-gluconate internal recording solution from 4–7 mice. Number of cells are in parentheses. Values are mean ± SE. C_m: cell membrane capacitance; R_m: input resistance; CsMe: cesium methanesulfonate internal recording solution.

Table 2. Fast spiking interneuron membrane properties of 8–9 month old zQ175 and WT mice.

		Cm (pF)	Rm (MΩ)
Sensory cortex			
8–9 months			
	zQ175 (6)	55.7 ± 11.0	291.5 ± 31.2
	WT (7)	47.2 ± 5.2	254.6 ± 34.0
Motor cortex			
8–9 months			
	zQ175 (6)	43.4 ± 11.4	276.4 ± 38.4
	WT (5)	40.9 ± 8.2	280.0 ± 25.9

Measurements were acquired using a K-gluconate internal recording solution from 4–5 mice. Number of cells are in parentheses. Values are mean ± SE. C_m: cell membrane capacitance; R_m: input resistance.

events have been recorded from R6/2 and YAC128 mouse brain slices, triggered by bicuculline or picrotoxin and consistent with eNMDAR-mediated activity [21, 23].

To further investigate mechanisms underlying aberrant cortical spread of sensory-induced activity found *in vivo*, here we record in acute cortical slices from zQ175 HD mice vs wildtype (WT) littermates to determine intrinsic neuronal excitability, quantify synaptic and network input in somatosensory CPNs and quantify fast-spiking interneurons (FSIs) electrophysiological properties at premanifest and early manifest disease stages. We contrast these results in the somatosensory cortex with those from motor cortex CPNs and INs, and reveal regional differences across the cortex. Results show reduced inhibitory drive coupled with increased large-amplitude excitatory network events in somatosensory cortex that may contribute to the previously reported enhanced spread of sensory cortex activity across regions.

Results

Basic membrane properties were similar between genotypes

Similar to the previously published electrophysiology study in motor cortex of zQ175 mice [24], we also report no significant age-dependent, genotype or regional differences in input resistance and capacitance of CPNs (Table 1). Likewise, no regional or genotype differences in input resistance and capacitance were seen in INs (Table 2) (see Methods for details on classification).

Intrinsic excitability and excitatory synaptic transmission of sensory cortical pyramidal neurons differ between genotypes in an age-dependent manner

Spontaneous excitatory postsynaptic currents (sEPSCs) were recorded in the voltage-clamp configuration at a holding potential of −70 mV from layer 2/3 (L2/3) CPNs in the somatosensory cortex of premanifest (3–4 month) and early-manifest (8–9 month) zQ175 and WT mice (Fig. 1A). No genotypic differences or change over time (from 3–4 to 8–9 months) were seen in sEPSC amplitude (Fig. 1B). However, at both 3–4 and 8–9 months sEPSC frequency was decreased in CPNs from zQ175 mice compared to WT (Fig. 1C). Within genotypes, no age-dependent changes in sEPSC frequency were seen. Most of the excitatory drive to these CPNs comes from intracortical connections; therefore, reduced excitatory synaptic transmission could, in part, be a result of reduced activity of afferents from other CPNs.

To directly examine CPN action potential firing, we next measured voltage responses to suprathreshold current-clamp step injection (Fig. 2). Overall, intrinsic excitability in zQ175 CPNs decreased as the mice progressed towards more behaviorally manifest ages, as defined in previous studies [26–28]. At 3–4 months, the rheobase of CPNs from zQ175 mice was reduced compared to WT CPNs (Fig. 2C). Numbers of action potentials fired in response to each current injection step above rheobase was also greater in CPNs from zQ175 mice (Fig. 2D). At 8–9 months, the opposite was true. CPNs from zQ175 mice at this age had a higher rheobase than CPNs from WT mice (Fig. 2C). The number

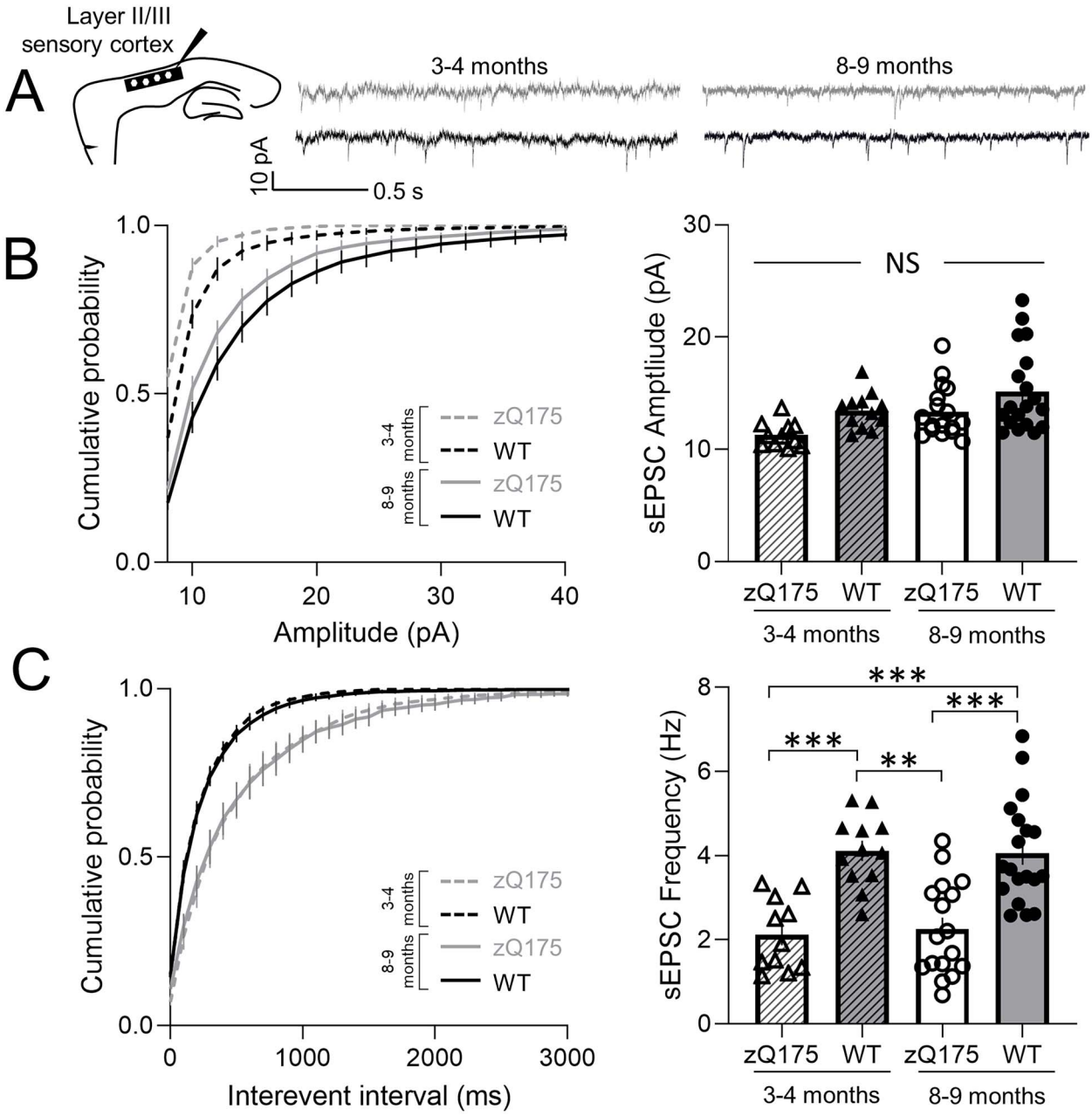

Figure 1. Excitatory synaptic transmission of sensory cortical pyramidal neurons is reduced in zQ175 mice. (A) Representative traces of spontaneous excitatory postsynaptic currents (sEPSCs) recorded from sensory cortical pyramidal neurons (CPNs) at 3–4 and 8–9 months for wildtype (WT) and zQ175 mice at a holding potential of −70 mV. (B and C) Cumulative probability of amplitude (B left panel) and frequency (C left panel) with corresponding mean amplitude (B right panel) and frequency (C right panel) (n = 11–19 from 4–5 mice for each group). Error bars denote SE. **, *** and NS denotes $P < 0.01$, 0.005 and statistically non-significant, respectively.

of action potentials fired in response to each current injection step above rheobase was also reduced in zQ175 CPNs (Fig. 2D). Examining age-dependent changes revealed that the rheobase of CPNs from zQ175 mice significantly increased over time (Fig. 2C). No age-dependent difference in rheobase was seen in WT mice. No genotypic differences or change over time were seen in the resting membrane potential (RMP) of somatosensory CPNs, suggesting changes in RMP do not underlie altered intrinsic excitability (Fig. 2B). Thus, intrinsic excitability of somatosensory CPNs from zQ175 mice surprisingly displayed biphasic age-dependent changes from hyper- to hypo-excitable.

Large-amplitude excitatory discharges recorded from sensory cortical pyramidal neurons are more prominent in HD mice

Previously published electrophysiology studies reported the presence of spontaneous large-amplitude excitatory discharges induced by $GABA_A$ receptor inhibition in both R6/2 and YAC128 mouse models [21, 23]. To investigate this phenomenon in zQ175 mice we examined picrotoxin (PTX)-induced spontaneous large-amplitude excitatory discharges from somatosensory CPNs at a holding potential of −70 mV (Fig. 3A). At 3–4 months, the percentage of CPNs with discharges was the same between zQ175

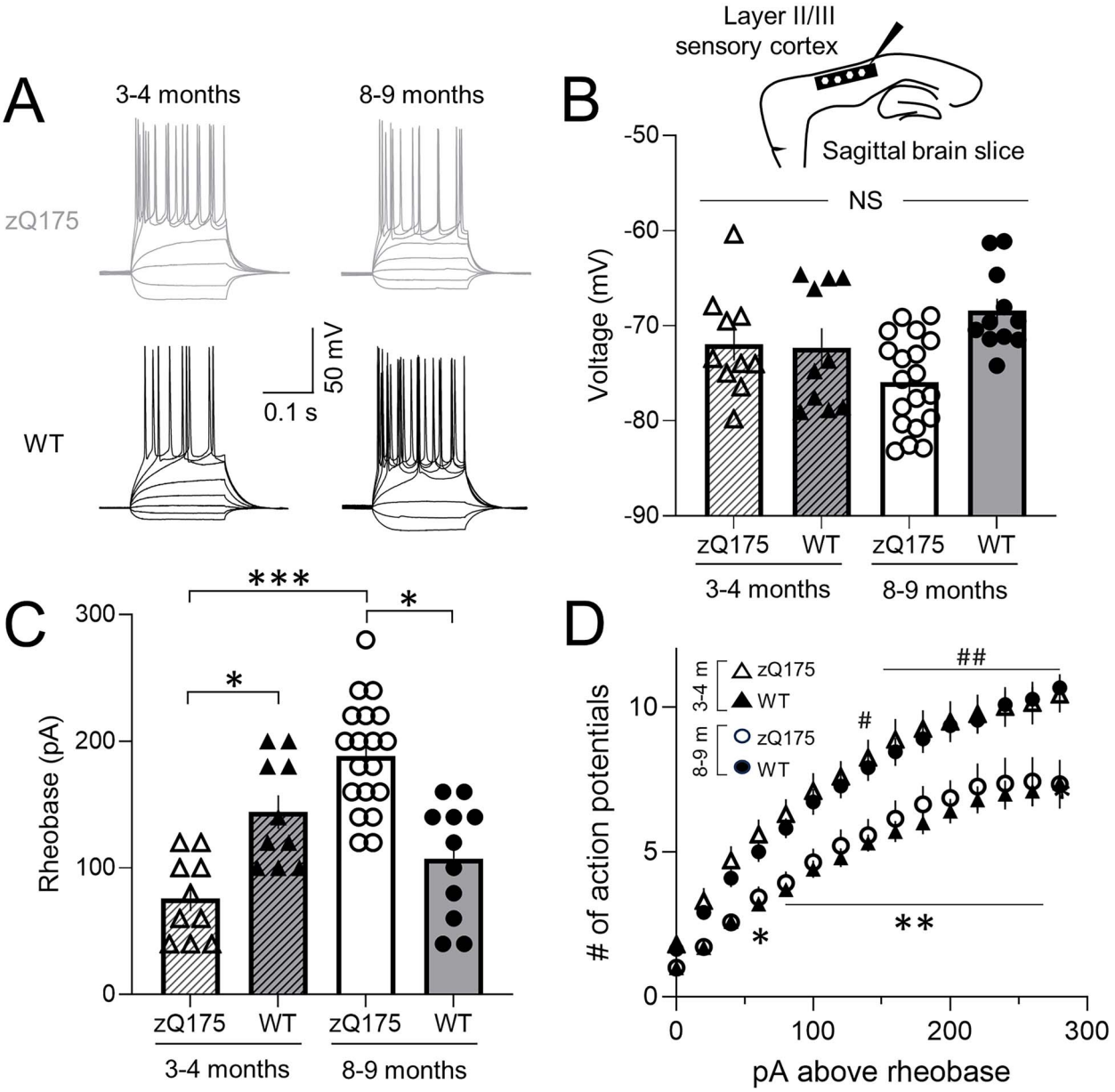

Figure 2. Intrinsic excitability of zQ175 sensory cortical pyramidal neurons decreases over time. (A) Representative traces of voltage responses to somatic current injections recorded from sensory cortical pyramidal neurons (CPNs) at 3–4 and 8–9 months for wildtype (WT) and zQ175 mice. (B–D) Resting membrane potential (B), rheobase (C) and number of action potentials as a function of depolarizing current injections above the rheobase (D) (# denotes statistical difference between 3–4 month (m) HD and 3–4 m WT; * denotes statistical difference between 8–9 m HD and 8–9 m WT) (3–4 m WT: solid triangles and zQ175: open triangles; 8–9 m WT: solid circles and zQ175: open circles) (n = 10–20 from 4–5 mice for each group). Error bars denote SE. * or #, ** or ##, *** and NS denotes $P < 0.05$, 0.01, 0.005 and statistically non-significant, respectively.

and WT mice (Fig. 3B). Although the percentage of CPNs with discharges decreased over time for both genotypes, this was more pronounced in WT mice. At 8–9 months, the percentage of zQ175 CPNs showing these discharges was significantly greater than that of WT CPNs. Moreover, zQ175 CPNs not only had a greater frequency of discharges at both ages compared to WT but the frequency of discharges also increased with age in zQ175 CPNs (Fig. 3C). No age-dependent changes in discharge frequency were apparent in WT CPNs.

Similar to [23] we also noted that some large-amplitude excitatory discharges could be further classified as complex (Fig. 3D). Complex discharges were defined as those that had multiple peaks (Fig. 3A, far right, top panel: first discharge results in a subsequent discharge before returning to baseline). Of the CPNs that displayed discharges, the percentage of zQ175 CPNs with complex discharges was greater than that of WT CPNs at both time points (Fig. 3D).

To confirm that zQ175 mice had an increased number of complex discharges compared to WT, we also examined the duration of discharges (Fig. 3E and F). Discharges included a fast inward component and a prolonged decay to baseline (Fig. 3A far right panels; dotted line shows baseline). Discharge duration was defined as the time required to return to baseline. In both age groups, CPNs from zQ175 mice had longer discharges compared to WT (Fig. 3E and F), consistent with the finding that zQ175 mice have increased complex discharges.

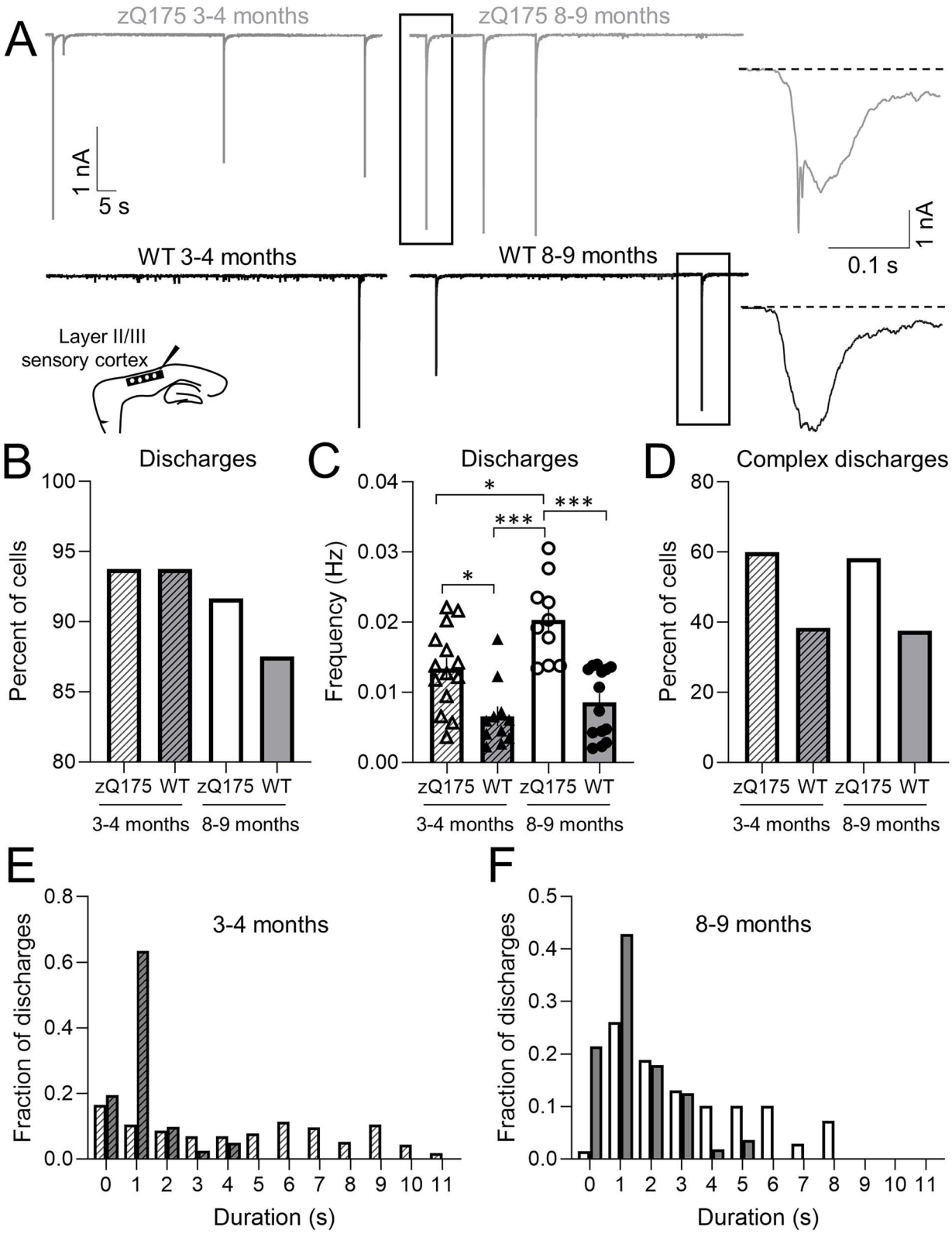

Figure 3. Large-amplitude excitatory discharges induced by picrotoxin are more frequent and complex in sensory cortical pyramidal neurons from zQ175 mice. (A) Representative large-amplitude excitatory discharges recorded from sensory cortical pyramidal neurons (CPNs) at 3–4 and 8–9 months for wildtype (WT) and zQ175 mice at a holding potential of −70 mV in the presence of 50 μM picrotoxin. (A, Insets) Expanded view of large-amplitude discharges showing slow decay to baseline (dotted line). (B–D) Percent of cells with discharges (B), discharge frequency (C) and percent of cells with complex discharges (D). (E and F) Distribution of discharge duration from 3–4 (E) and 8–9 (F) month WT and zQ175 mice (n = 10–14 from 4–5 mice for each group). Error bars denote SE. *, *** and NS denotes $P < 0.05$, 0.005 and statistically non-significant, respectively.

Increased excitability of motor cortex pyramidal neurons reveals genotype changes are regionally specific

A previously published report of *ex vivo* cortical electrophysiology in 2- and 12-month old zQ175 mice, conducted in the motor cortex, found no difference in excitatory input at either early (pre-manifest) or late stages [24], which contrasts our above findings in sensory cortex CPNs. We therefore also examined intrinsic excitability and excitatory synaptic transmission of CPNs from the motor cortex of 8–9 month old (early-manifest) mice (Fig. 4A). In contrast to the reduced excitatory input onto sensory CPNs, the sEPSC frequency was increased in motor CPNs from zQ175 mice compared to WT (Fig. 4C), suggesting zQ175 motor cortex CPNs are hyper-excitable at this early-manifest stage. No genotype differences in sEPSC amplitude were seen (Fig. 4B).

The current-clamp configuration revealed no genotype differences in RMP (Fig. 4D left panel). Although the number of action potentials fired in response to each current injection step above rheobase was not different between genotypes (Fig. 4E), the rheobase of zQ175 motor CPNs was reduced compared to WT (Fig. 4D right panel). CPNs in the motor cortex of zQ175 mice therefore had increased intrinsic excitability at the early-manifest stage compared to WT, distinct from the hypo-excitability of sensory CPNs at this age.

In addition, the percentage of zQ175 motor CPNs with large-amplitude excitatory discharges (see examples in Fig. 5A) was greater compared to WT (Fig. 5B). The percentage of motor CPNs with complex discharges was also increased in zQ175 mice (Fig. 5D). Consistent with this, discharges in zQ175 motor CPNs had a longer duration compared to WT (Fig. 5E). The frequency of discharges however, was not genotypically different in the motor cortex (Fig. 5C) unlike in the somatosensory cortex where more frequent discharges were apparent in zQ175 mice (Fig. 3C). Regional differences in large-amplitude discharge frequency may therefore impact compensatory mechanisms and contribute, at least in part, to the differences in excitability across the sensorimotor cortex.

Enhanced excitatory-inhibitory (E-I) balance in somatosensory cortical pyramidal neurons of early-manifest Q175 mice

Inhibitory neuron (IN) activity is critical to determining network spread of cortical excitability. To directly explore IN intrinsic excitability, recordings were made in current-clamp from fast-spiking INs (FSIs) (Fig. 6) of early-manifest (8–9 month) zQ175 and WT mice. FSIs were identified based on their low capacitance (Table 2), shorter spike half-width and higher maximal firing frequency (FF) compared to CPNs (Fig. 6B and C) [29]. No genotype differences in basic membrane properties (Table 2) and RMP (Fig. 6D and G) of FSIs were seen in either cortical region. In the somatosensory cortex, FSIs from zQ175 mice had a higher rheobase (Fig. 6E) and fired significantly fewer action potentials in response to each current injection step above rheobase (Fig. 6F) compared to FSIs from WT mice. In contrast, no genotype differences in rheobase (Fig. 6H) or the number of action potentials fired (Fig. 6I) were apparent for FSIs recorded in the motor cortex. FSIs in the somatosensory cortex but not the motor cortex of zQ175 mice are therefore hypo-excitable, suggesting regional differences in inhibitory drive across the cortex.

To investigate whether somatosensory FSI intrinsic hypo-excitability is associated with altered inhibitory input onto CPNs, we first recorded spontaneous inhibitory postsynaptic currents (sIPSCs) in the voltage-clamp configuration at a holding potential of +10 mV from somatosensory CPNs of early-manifest (8–9 month) zQ175 and WT mice (Fig. 7A–C). No genotype differences were seen in sIPSC amplitude (Fig. 7B). sIPSC frequency however, was decreased in CPNs from zQ175 mice compared to WT (Fig. 7C). To understand whether these changes could shift the somatosensory cortical network towards net hyper-excitability, we turned our attention to the excitatory-inhibitory (E-I) balance. We stimulated layer 4 neurons, which are known to send excitatory inputs to both CPNs and interneurons in layer 2/3. Recording from layer 2/3 CPNs, we assessed the ratio between excitatory and inhibitory inputs (E-I ratio) at −70 mV and +10 mV holding potentials (Fig. 7D). The inhibitory inputs to layer 2/3 CPNs recorded at +10 mV following layer 4 stimulation are di-synaptic, and the dependency of these responses on AMPA receptor (AMPAR) and $GABA_AR$ activation was confirmed through successful blockade with CNQX and picrotoxin (Fig. 7E). Interestingly, our findings reveal a higher E-I ratio in zQ175 mice compared to WT in the somatosensory cortex (Fig. 7F), indicating an alteration in the feedforward inhibition within this cortical circuitry.

Discussion

Transcranial magnetic stimulation studies in premanifest and early HD patients have revealed changes in cortical excitation and inhibition [30, 31] necessitating further understanding of early cellular mechanisms of HD. Critical translational parallels can be made from electrophysiological studies that use HD mouse models with increasingly better face, construct and predictive validity. Here we report regional, cell-type and age-dependent differences in zQ175 cortical excitability, revealing enhanced E-I balance in somatosensory cortex that may contribute to previously published aberrant spread of sensory stimulation-induced cortical activity *in vivo* [21]. Moreover, the age- and region-dependent changes in intrinsic excitability, as well as excitatory and inhibitory inputs of somatosensory CPNs, may reflect an attempt at compensation for early, excessive excitation that could contribute to eventual neurodegenerative changes in HD.

Somatosensory cortex excitability

Early fine motor incoordination manifests in zQ175 mice at ∼6 months of age [32], whereas, gross motor phenotype manifestations occur at ∼9 months or later [32–35]. Moreover, an aberrant spread of sensory stimulation-induced cortical activity was observed in ∼7 month-old zQ175 mice [21]. Therefore, our *ex vivo* electrophysiology experiments in the somatosensory cortex included a premanifest (3–4 months) and early-manifest (8–9 months) time point to assess pathophysiological progression.

Excitatory synaptic transmission in the somatosensory cortex has previously been characterized for R6/2, YAC128 and CAG140 mice [23] but not zQ175 mice. In contrast to that study, which reported an increase in sEPSC frequency in CPNs from other HD mouse models at the motor manifest stage, we saw a decrease in frequency in somatosensory cortex CPNs from both premanifest and early-manifest zQ175 mice. Aside from the model used, the difference in results could be explained, in part, by differences in internal and external recording solutions: the previous study [23] recorded sEPSC frequency using a cesium-based internal solution that facilitated detection of small events in distal dendrites, whereas we measured sEPSCs with a potassium-based internal, which would unmask any differences in shunt conductances between genotypes. As well, Cummings and colleagues made

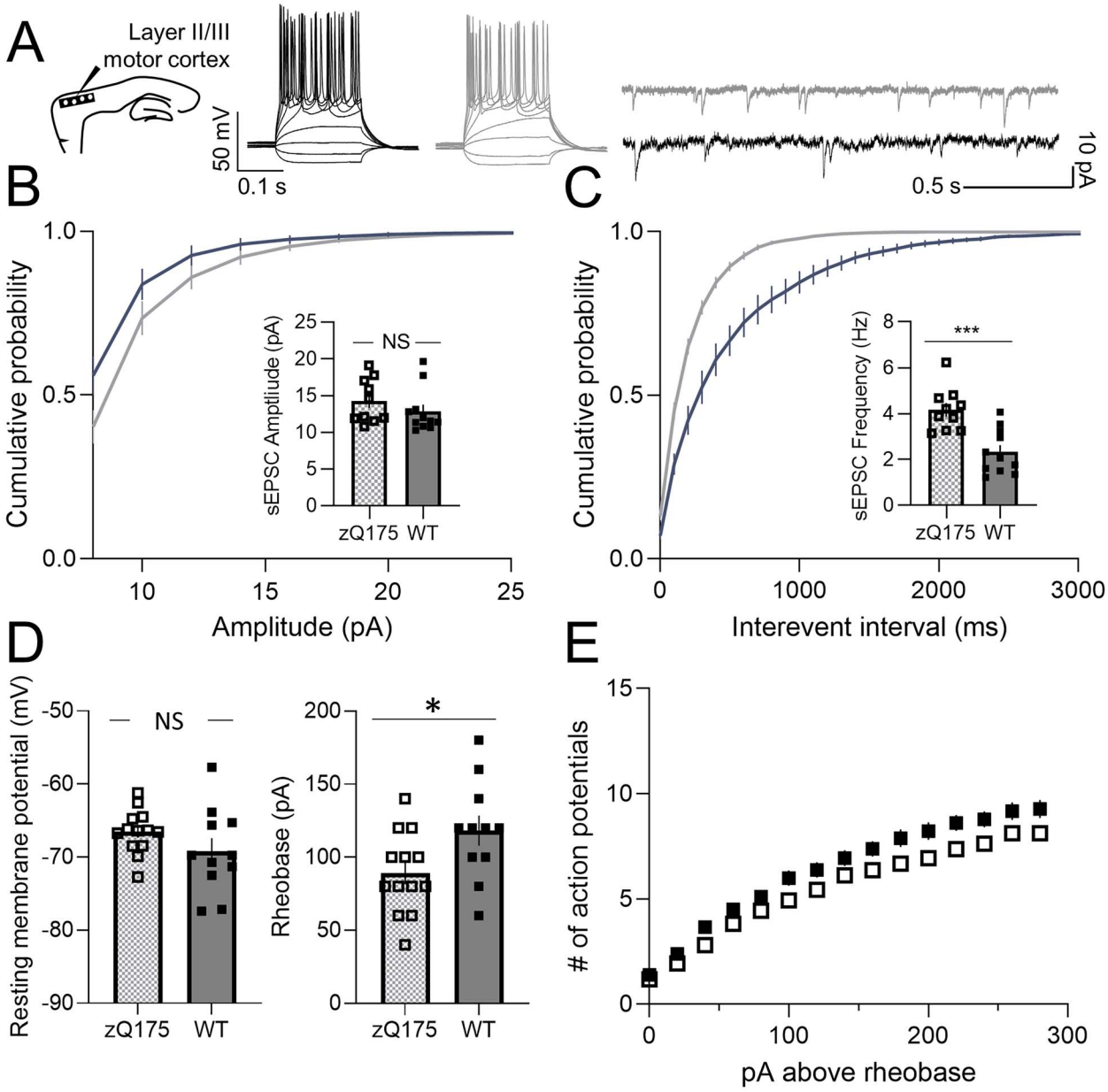

Figure 4. Increased excitability in motor cortical pyramidal neurons from 8–9 month zQ175 mice. (A) Representative traces of voltage responses to somatic current injections (left panel) and spontaneous excitatory postsynaptic currents (sEPSCs; right panel) recorded from motor cortical pyramidal neurons (CPNs) at 8–9 months for wildtype (WT) and zQ175 mice. (B and C) Cumulative probability of amplitude (B) and frequency (C) zQ175 and WT with corresponding mean amplitude and frequency shown in insets (n = 10–11 from 4–5 mice for each group). (D–E) Resting membrane potential (D left panel), rheobase (D right panel) and number of action potentials as a function of depolarizing current injections above the rheobase (E) (n = 11–13 from 4–5 mice for each group). Error bars denote SE. *, *** and NS denotes $P < 0.05$, 0.005 and statistically non-significant, respectively.

most of their recordings in the presence of the $GABA_A$ receptor inhibitor bicuculline, whereas the external solution used in our experiments lacked any $GABA_AR$ blockade; removing inhibition with bicuculline would increase excitability in the slice and the frequency of sEPSCs. The decrease in sEPSC frequency found in our study does not appear to be a result of reduced CPN action potential frequency at least at the premanifest stage, since somatosensory CPNs from premanifest zQ175 mice showed increased intrinsic excitability (reduced rheobase and greater action potential firing in response to current steps). Two alternative presynaptic alterations that could explain this reduction in sEPSC frequency include a decrease of release sites (number of CPN-CPN synapses) or probability of neurotransmitter release from CPN terminals. Since morphological alterations have not been reported in zQ175 motor cortex CPNs at 2 and 12 months of age [24], it is likely that a reduction in release probability could explain our results in somatosensory cortex CPNs from premanifest zQ175 mice.

In the early-manifest stage, although sEPSC frequency was still reduced in zQ175 somatosensory CPNs, surprisingly so was the intrinsic excitability (increased rheobase and reduced action potential firing in response to current steps), suggesting either a decrease in release probability or action potential frequency. Loss of the ability to sustain action potential firing has also previously been reported in the perirhinal cortex of late stage R6/1 mice (7 months) [36]. We postulate that reduced intrinsic excitability

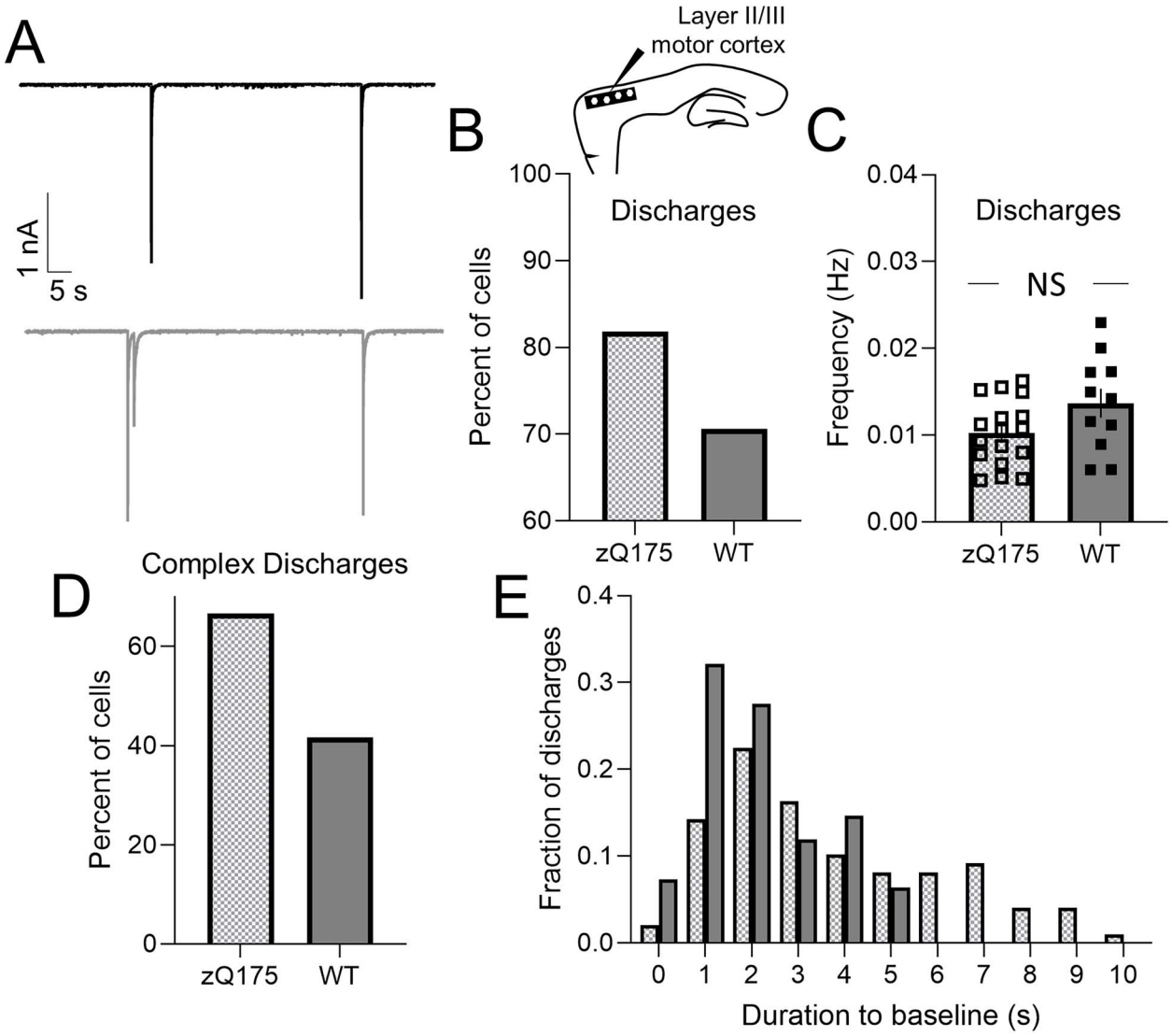

Figure 5. Large-amplitude discharges induced by picrotoxin are more complex in motor cortical pyramidal neurons from zQ175 mice. (A) Representative large-amplitude discharges recorded from motor cortical pyramidal neurons (CPNs) at 8–9 months for wildtype (WT) and zQ175 mice at a holding potential of −70 mV in the presence of 50 μM picrotoxin. (B and D) Percent Of cells with discharges (B), discharge frequency (C) and percent of cells with complex discharges (D). (E) Distribution of the duration of discharges from 8–9 month WT (solid bars) and zQ175 mice (checkered bars) (n = 11–17 from 4–5 mice for each group). Error bars denote SE. NS denotes statistically non-significant.

of somatosensory CPNs may reflect a later-stage change in response to cortical hyper-excitability at earlier stages of HD. Consistent with this hypothesis, an age-dependent increase then decrease in calcium transient frequency (reflective of CPN firing rate) has also been observed in *in vivo* calcium imaging studies of the motor cortex, comparing 2–3 month with 12–18 month zQ175 and WT mice [37]. It is interesting that in 8–9 month zQ715 somatosensory CPNs we found an increase in rheobase and reduction in action potential firing in current clamp without an associated change in resting membrane potential or input resistance (measured at RMP); a variety of voltage-dependent K^+ channels, including those that are also gated by Ca^{2+}, could be altered in their activity to contribute to enhanced K^+ shunt conductance upon depolarization. These possibilities could be explored in future experiments. Overall, the biphasic change in intrinsic excitability from hyper- to hypo-excitable suggests the cortex undergoes progressive changes.

Motor cortex excitability

Unlike the somatosensory cortex, excitatory and inhibitory synaptic transmission in the motor cortex of zQ175 mice has been characterized at the premanifest (2 months) and manifest stage (12 months) [24]. We therefore concentrated on the early-manifest stage (8–9 months) and also examined regional differences between the somatosensory and motor cortices. Although no genotypic differences in sEPSC frequency were reported at 2 and 12 months of age in motor cortex CPNs [24], we saw an increase in sEPSC frequency and a decrease in rheobase indicating that age-dependent changes also take place in the motor cortex, where CPNs show hyper-excitability at this early motor-manifest stage. If hypo-excitability found in the sensory cortex at 8–9 months is a response to earlier stage increased excitatory drive, then the hyper-excitability we found in the motor cortex suggests differences in the rate of disease progression across the cortex. Consistent with this hypothesis, regional differences in

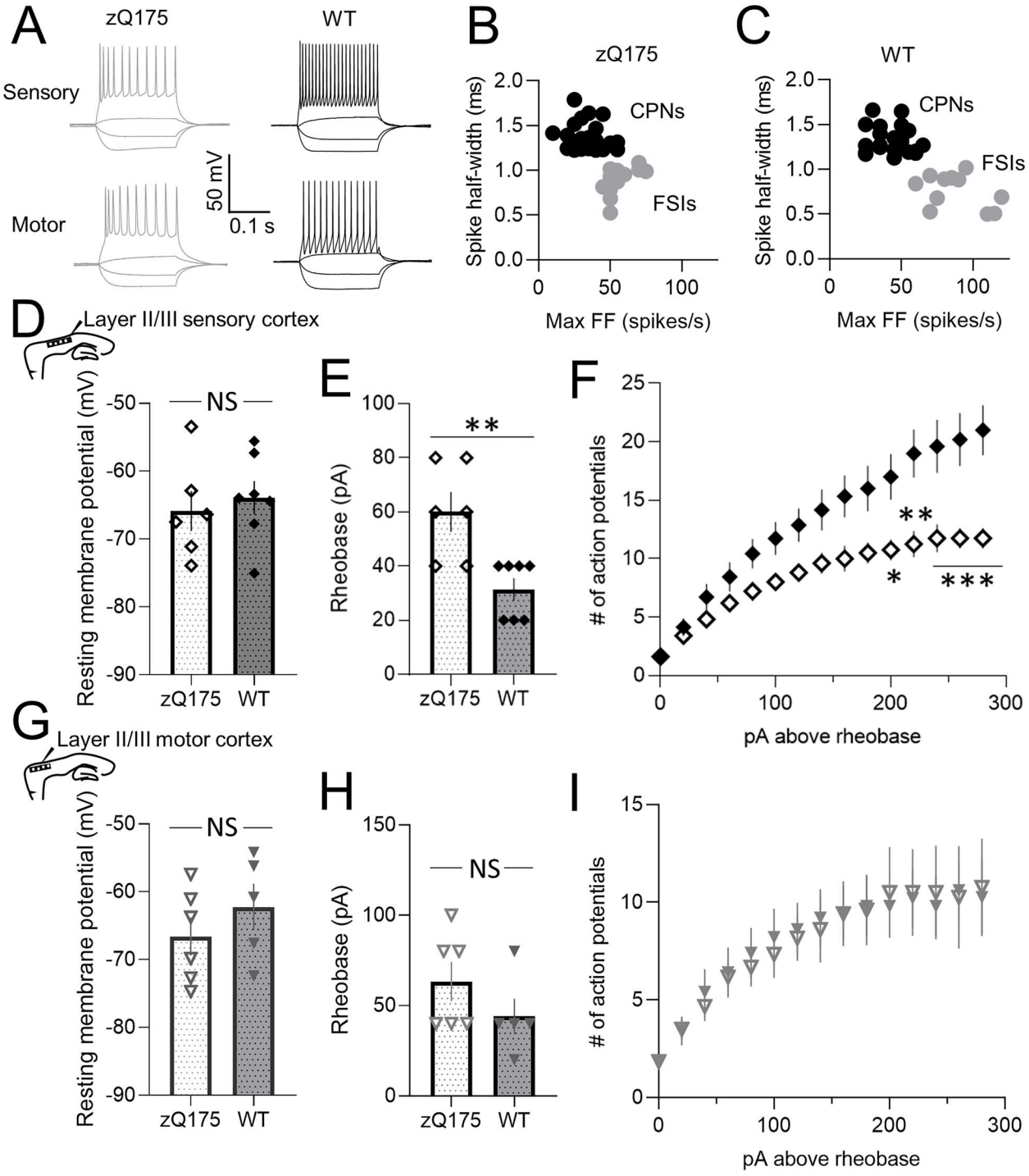

Figure 6. Reduced fast-spiking interneuron intrinsic excitability in the sensory but not motor cortex of zQ175 mice at 8–9 months. (A) Representative traces of voltage responses to somatic current injections recorded from sensory (top panels) and motor (bottom panels) fast-spiking interneurons (FSIs) at 8–9 months for wildtype (WT) and zQ175 mice. (B and C) CPN and FSI spike half-width as a function of maximal firing frequency (FF) from zQ175 (B) and WT (C) mice. (D–I) Resting membrane potential (D and G) and rheobase (E and H) from sensory (D and E) (n = 6–7 (4–5 mice) per group) and motor (G and H) (n = 5–6 (4–5 mice) per group) FSIs. Number of action potentials as a function of depolarizing current injections above the rheobase from sensory (F) and motor (I) FSIs (zQ175: open diamond or triangle; WT: solid diamond or triangle). Error bars denote SE. *, **, *** and NS denotes $P < 0.05$, 0.01, 0.005 and statistically non-significant, respectively.

HD progression have been reported in clinical MRI studies [38]. HD patients with a higher CAG-repeat length were reported to show an increased rate of atrophy especially in the posterior cortical areas, including the postcentral but not precentral gyrus, suggesting the somatosensory cortical areas may be more vulnerable.

Regional differences in cortical large-amplitude excitatory discharges

We speculate that the switch to reduced intrinsic CPN excitability in the somatosensory cortex may, in part, be explained by robust changes in excitatory network activity. Similar to other studies [21, 23, 39], we also report the presence of large-amplitude excitatory

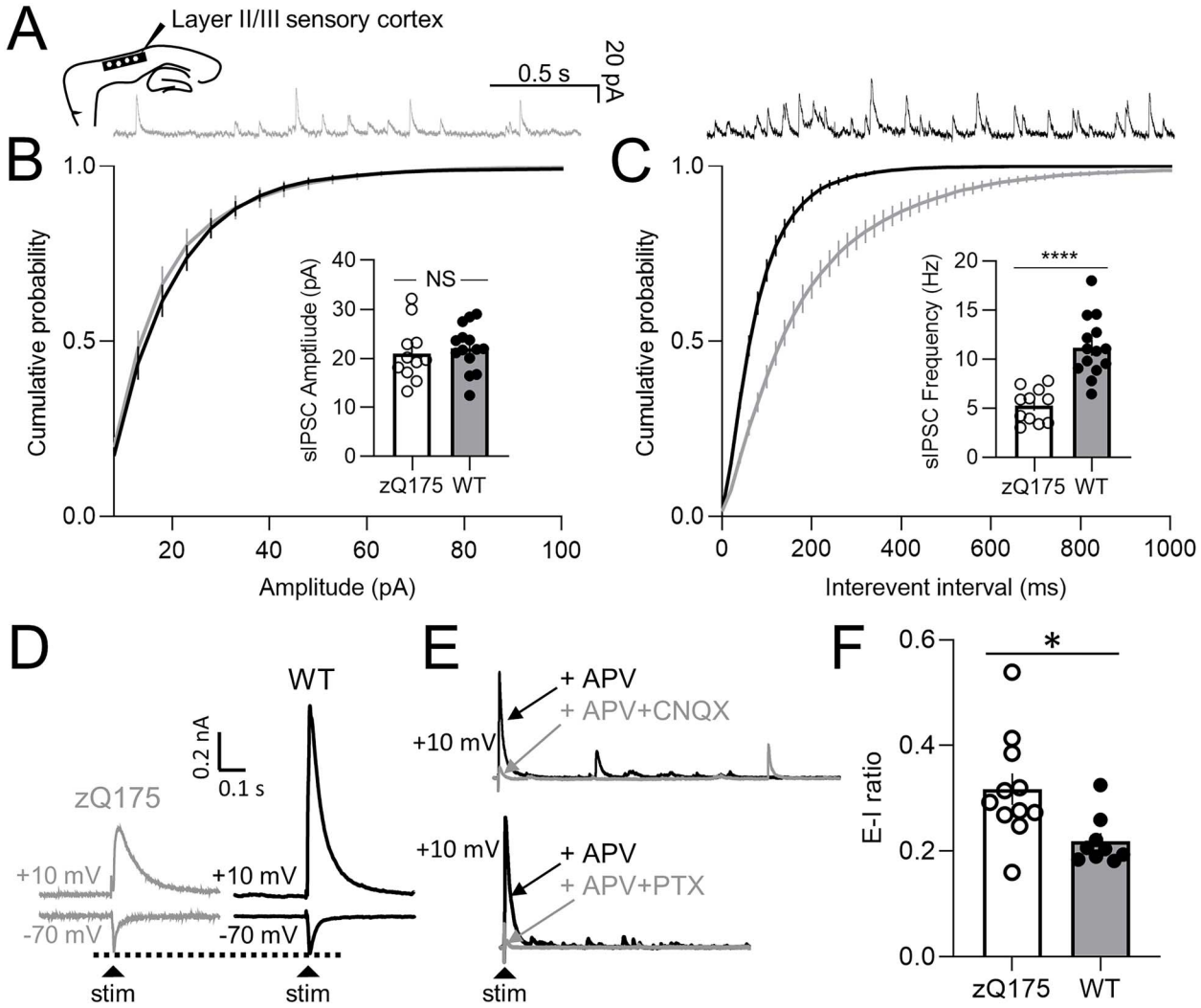

Figure 7. Inhibitory synaptic input is reduced and excitatory-inhibitory (E-I) ratio is larger in the sensory cortex of 8–9 month zQ175 mice. (A) Representative traces of spontaneous inhibitory postsynaptic currents (sIPSCs) recorded from sensory cortical pyramidal neurons (CPNs) at 8–9 months for wildtype (WT) and zQ175 mice at a holding potential of +10 mV. (B and C) Cumulative probability of sIPSC amplitude (B) and frequency (C) with corresponding mean amplitude and frequency shown in insets (n = 11–14 (3–4 mice) per group). (D–F) All excitatory-inhibitory ratio experiments were conducted in the presence of 50 μM D-APV. (D) Representative evoked excitatory postsynaptic current (eEPSC) recorded at a holding potential of −70 mV, and evoked inhibitory postsynaptic current (eIPSC) recorded at a holding potential of +10 mV from layer II/III sensory CPNs in response to stimulation in layer IV. (E) Representative blockade of eIPSC after treatment with 10 μM CNQX (upper panel) or 50 μM picrotoxin (PTX) (lower panel). (F) E-I ratio of layer II/III sensory CPNs (n = 9–11 (3 mice) per group). Error bars denote SE. * denotes $P < 0.05$.

discharges in the somatosensory and motor cortices. Although we have not directly identified the specific ion channel underlying these large discharges, evidence from other studies suggests an involvement of eNMDA receptors. In a recent study, we showed that these discharges can also be recorded from layer 2/3 CPNs by stimulating layer 4 and voltage-clamping the CPNs at +40 mV in the presence of AMPA and $GABA_A$ receptor blockers [21]. Subsequent TBOA treatment, which enhances eNMDAR current by blocking glutamate clearance, increased these large-amplitude discharges. Other HD mouse models show large complex events recorded at negative holding potentials in the striatum and cortex that are more prevalent than in WT mice after TBOA treatment [39, 40]. These studies suggest that spontaneous network events may also be triggered, in part, by deficits in glutamate clearance by astrocytes [39, 41].

In the somatosensory cortex, although the frequency and complexity (duration) of discharges was increased in zQ175 somatosensory CPNs at both premanifest and early-manifest stages, the increase in frequency became more significant with disease progression. Given that eNMDAR overactivation induces neuronal death through sustained neuronal membrane depolarization, augmented Ca^{2+} influx and mitochondrial dysfunction [42], the hypo-excitability of somatosensory CPNs at the early-manifest stage may be a protective mechanism to mitigate these excitotoxic effects. In the motor cortex of zQ175 mice, although large-amplitude discharges recorded from CPNs are more complex compared to WT, there was no genotype difference in discharge frequency, suggesting a reduced need to undergo compensatory changes in this cortical region at this age, which may help explain the regional differences in CPN excitability across the sensorimotor cortex.

Regional differences in inhibitory drive

Cortical excitability has also been attributed to reduced inhibitory drive. Differences in sIPSC frequency have been reported across

stages, models and cortical regions [23, 25]. zQ175 mice display significantly reduced inhibitory drive in motor cortex by 12 months [24]; similarly, BACHD mice showed a decrease in sIPSC frequency [25]. Consistent with these findings, we also report a decrease in sIPSC frequency recorded from CPNs in the somatosensory cortex of early-manifest (8–9 month) HD mice. Our finding of increased E-I ratios in somatosensory CPNs from these early-manifest HD mice further supports the hypothesis of cortical hyper-excitability. Although the reduced frequency of sIPSCs may reflect, in part, a direct effect of mutant HTT in cortical INs, it is also possible that CPN intrinsic hypo-excitability triggers a compensatory reduction in inhibitory input [43]. Either way, the reduced local inhibition could then exacerbate spread of excitatory network activity in response to strong stimuli from thalamic afferents (through layer 4), as well as augment the generation and/or network spread of large-amplitude excitatory discharges mediated, in part, by eNMDAR [21], in a positive feedback loop with net increase in E-I balance. This model is consistent with the idea that reduced sIPSC frequency and increased E-I ratio originates from local GABA-ergic INs [19, 25, 44]. Notably, we found decreased intrinsic excitability in zQ175 somatosensory but not motor cortical INs, consistent with the absence of intrinsic hypo-excitability of motor cortex CPNs. We speculate that the motor cortex could display compensatory intrinsic hypo-excitability at later disease stages following cortical hyper-excitability.

Previously, we reported enhanced sensory spread in YAC128 and zQ175 mice using voltage-sensitive dye imaging and multi-electrode recording *in vivo* [21]. Our current observations suggest a nuanced interplay between local and global network alterations in the context of HD. This greater sensory spread could be explained by the increased frequency of large-amplitude eNMDAR-mediated excitatory network discharges combined with reduced inhibitory drive in the somatosensory cortex. The observed intrinsic hypo-excitability of somatosensory CPNs, while seemingly counterintuitive, may be viewed as part of a dynamic equilibrium aimed at mitigating excessive excitation within the network. This could represent a homeostatic compensatory mechanism whereby local neuronal excitability and global network activity interact, in an attempt to maintain a functional balance in response to the pathophysiological alterations induced by the disease process. To substantiate this hypothesis, a deeper exploration into the bidirectional interaction between individual neuronal properties and network-level dynamics, encompassing a multiscale approach, is warranted. The elucidation of these intricate mechanisms could pave the way for novel therapeutic interventions aimed at re-establishing the delicate equilibrium within these neuronal networks.

Conclusion

In summary, although the zQ175 HD mouse model offers the best construct validity, little was previously known about the dynamic changes in excitability which occur across the cortex throughout disease progression. Taken together, we demonstrate for the first time, regional- and age-dependent differences in intrinsic excitability across the sensorimotor cortex, which we speculate could be explained by compensatory mechanisms against cortical hyper-excitability, the latter mediated by enhanced eNMDAR-mediated network events and aberrant inhibitory drive from INs resulting in an increased E-I ratio. In patients with HD, both region- and symptom-dependent loss of cortical INs has previously been reported [45], highlighting the importance of INs in HD. Our study further suggests that the role of FSIs and other types of GABA-ergic INs should be first characterized using expression of optogenetic markers to label specific IN subpopulations, then targeted in the future as a potential therapeutic approach to regulate progressive changes in HD excitability and phenotype.

Materials and Methods

Animals

All experiments and procedures were carried out in accordance with the Canadian Council on Animal Care and approved by the University of British Columbia Committee on Animal Care (protocols A23-0083, A21-0276). Animal tissue was collected through ear clipping at weaning. DNA extraction and PCR analysis were subsequently used to determine genotype. Experiments were performed on equal number of male and female heterozygous zQ175DN knock-in C57BL/6 (zQ175) mice and wildtype (WT) littermates as controls at either 3–4 (premanifest) or 8–9 (early-manifest) months of age. Only zQ175 mice with a CAG repeat length of 180–200 were used for experiments. No differences were observed between sexes. Data from both sexes were therefore combined.

Solutions, drugs and slice preparation

Unless otherwise stated, all drugs and chemicals used to make solutions were obtained from Sigma-Aldrich (Mississauga, ON, Canada). Animals were first anesthetized with isoflurane vapor, then decapitated and finally, their brains rapidly removed. Sagittal brain slices (250 μm) were cut using a Leica VT1000 vibratome in ice-cold low calcium artificial cerebrospinal fluid (aCSF; with 0.5 mM $CaCl_2$ and 2.5 mM $MgCl_2$) containing 1 mM Kynurenic acid equilibrated with 95% O_2–5% CO_2. Motor and sensory cortex slices containing the striatum were transferred and incubated in a holding chamber with oxygenated aCSF (125 mM NaCl, 2.5 KCl mM, 25 mM $NaHCO_3$, 1.25 mM NaH_2PO_4, 1 mM $MgCl_2$, 2 mM $CaCl_2$, 10 mM glucose, pH 7.3–7.4, 310–314 mOsm) at 37°C for 45 min then maintained at room temperature before recording. In the recording chamber, slices were continuously superfused at room temperature with oxygenated aCSF with or without 50 μM picrotoxin (PTX) (Tocris Bioscience, Oakville, ON, Canada) or 50 μM 2-amino-5-phosphonovaleric acid (D-APV) (Tocris Bioscience, Oakville, ON, Canada). Recording pipettes (3–5 MΩ) were made from borosilicate glass capillaries using a Narishige micropipette puller (Narishige International) and filled with a K-gluconate internal recording solution (122 mM K-gluconate, 13 mM KCl, 0.3 mM EGTA, 4 mM MgATP, 0.3 mM NaGTP, 10 mM HEPES, 10 mM Na-phosphocreatine, pH 7.35 using KOH, osmolarity 290 mOsm) for all experiments except for spontaneous inhibitory postsynaptic currents (sIPSCs) and excitatory-inhibitory (E-I) ratio experiments where a CsMe internal recording solution was used (130 mM CsMe, 5 mM CsCl, 4 mM NaCl, 1 mM MgCl2, 10 mM HEPES, 5 mM EGTA, 5 mM QX-314Cl, 0.5 mM NaGTP, 10 mM Na-phosphocreatine, 5 mM MgATP at pH 7.3 and 290 mOsm). aCSF was used to fill the stimulating pipette.

Electrophysiology

A Multiclamp 700A amplifier, Axon Digidata 1550B digitizer and Clampex 10.7 were used to acquire all whole-cell patch clamp recordings from layer II/III neurons. All recordings were digitized at 20 kHz and low pass filtered at 1 kHz for voltage-clamp (holding potential of +10 mV for sIPSCs and −70 mV for both

spontaneous excitatory postsynaptic currents (sEPSCs) and large-amplitude excitatory discharge recording) and 2 kHz for current-clamp experiments using an analogue Bessel filter. A threshold of 8 pA was used for sEPSCs and sIPSCs. Large-amplitude excitatory discharges were induced by treatment with 50 μM PTX [21, 23]. Complex discharges were defined as those that had multiple peaks (see Fig. 3A top left panel). Duration of discharges were quantified as the time of discharge initiation until return to baseline (see Fig. 3A inset panels for enlarged view depicting slow decay to baseline (dotted line)). Current-clamp configuration was used to determine resting membrane potential (RMP), rheobase and action potential firing (total number of action potentials as a function of depolarizing current injections above the rheobase). Protocol consisted of somatic current injections for 200 ms, starting at −100 pA and incremented by 20 pA steps with an interpulse interval of 10 s. Presumed GABA-ergic interneurons (INs) [46] were identified by their low capacitance (Table 2), as well as their shorter spike half-width and higher maximal firing frequency (FF) compared to CPNs, as previously described in [29](Fig. 6B and C). To determine the excitatory-inhibitory (E-I) ratio, evoked (monosynaptic) EPSCs (eEPSCs) and evoked (disynaptic) IPSCs (eIPSCs) were recorded at −70 mV and +10 mV, respectively from layer II/III sensory CPNs in response to stimulation in layer IV in the presence of 50 μM D-APV in the external bath solution to block NMDAR currents. The E-I ratio was subsequently determined by dividing the peak of the eEPSC by the peak of the eIPSC. 10 μM CNQX disodium salt (Tocris Bioscience, Oakville, ON, Canada) or 50 μM PTX was used in the external bath solution to confirm the recording of disynaptic $GABA_AR$-mediated current at a holding potential of +10 mV.

Data analysis

Clampfit 10.7 (Axon Instruments) and GraphPad Prism 9.3.1 were used to analyze all the data. Two-way Anova followed by the *Šídák* multiple comparison post-hoc test or student two-tailed *t*-test was used to determine statistical significance (as indicated in figure legends). A minimum of 3 mice per group was used (Figure Legends denote the number of cells recorded: "n"). A *P*-value less than 0.05 was considered statistically significant. All data in the figures and tables are mean ± SE (standard error).

Author contributions

Y.W., D.R., M.D.S., J.P.M. and L.A.R. designed the experiments. Y.W. and D.R. performed the research. Y.W. and D.R. analyzed the data, and M.D.S., J.P.M. and L.A.R. contributed to data interpretation. Y.W. drafted the manuscript with input and editing from D.R., M.D.S., J.P.M. and L.A.R.

Conflict of interest statement: The authors declare no competing financial interests.

Funding

We thank Lily Zhang for technical genotyping assistance. This work was supported by resources made available through the Canadian Institutes of Health Research [FDN 143210 and PJT 178043 to L.A.R.]. For a portion of this work Y.W. was supported by the Vanier Canada Graduate Scholarship and UBC's Four-Year Doctoral Fellowship. J.P.M. was supported by a Fellowship from the Hereditary Disease Foundation.

Data availability

All data are available upon reasonable request.

References

1. MacDonald ME, Ambrose CM, Duyao MP. *et al.* A novel gene containing a trinucleotide repeat that is expanded and unstable on Huntington's disease chromosomes. *Cell* 1993;**72**:971–83.
2. Cepeda C, Levine MS. Synaptic dysfunction in Huntington's disease: lessons from genetic animal models. *Neuroscientist* 2022;**28**:20–40.
3. Tabrizi SJ, Ghosh R, Leavitt BR. Huntingtin lowering strategies for disease modification in Huntington's disease. *Neuron* 2019;**102**:899.
4. Molero AE, Arteaga-Bracho EE, Chen CH. *et al.* Selective expression of mutant huntingtin during development recapitulates characteristic features of Huntington's disease. *Proc Natl Acad Sci U S A* 2016;**113**:5736–41.
5. Raymond LA, André VM, Cepeda C. *et al.* Pathophysiology of Huntington's disease: time-dependent alterations in synaptic and receptor function. *Neuroscience* 2011;**198**:252–73.
6. Barry J, Bui MTN, Levine MS. *et al.* Synaptic pathology in Huntington's disease: beyond the corticostriatal pathway. *Neurobiol Dis* 2022;**162**:105574.
7. Plotkin JL, Surmeier DJ. Corticostriatal synaptic adaptations in Huntington's disease. *Curr Opin Neurobiol* 2015;**33**:53–62.
8. Milnerwood AJ, Gladding CM, Pouladi MA. *et al.* Early increase in extrasynaptic NMDA receptor signaling and expression contributes to phenotype onset in Huntington's disease mice. *Neuron* 2010;**65**:178–90.
9. Milnerwood AJ, Kaufman AM, Sepers MD. *et al.* Mitigation of augmented extrasynaptic NMDAR signaling and apoptosis in cortico-striatal co-cultures from Huntington's disease mice. *Neurobiol Dis* 2012;**48**:40–51.
10. Kovalenko M, Milnerwood A, Giordano J. *et al.* $Htt^{Q111/+}$ Huntington's disease knock-in mice exhibit brain region-specific morphological changes and synaptic dysfunction. *J Huntingtons Dis* 2018;**7**:17–33.
11. Botelho EP, Wang E, Chen JY. *et al.* Differential synaptic and extrasynaptic glutamate-receptor alterations in striatal medium-sized spiny neurons of aged YAC128 Huntington's disease mice. *PLoS Curr* 2014;**6**:ecurrents.hd.34957c4f8bd7cb1f5ec47381dfc811c3. https://doi.org/10.1371/currents.hd.34957c4f8bd7cb1f5ec47381dfc811c3.
12. Plotkin JL, Day M, Peterson JD. *et al.* Impaired TrkB receptor signaling underlies corticostriatal dysfunction in Huntington's disease. *Neuron* 2014;**83**:178–88.
13. Dau A, Gladding CM, Sepers MD. *et al.* Chronic blockade of extrasynaptic NMDA receptors ameliorates synaptic dysfunction and pro-death signaling in Huntington disease transgenic mice. *Neurobiol Dis* 2014;**62**:533–42.
14. Reiner A, Dragatsis I, Dietrich P. Genetics and neuropathology of Huntington's disease. *Int Rev Neurobiol* 2011;**98**:325–72.
15. Rosas HD, Liu AK, Hersch S. *et al.* Regional and progressive thinning of the cortical ribbon in Huntington's disease. *Neurology* 2002;**58**:695–701.
16. Rosas HD, Salat DH, Lee SY *et al.* Cerebral cortex and the clinical expression of Huntington's disease: complexity and heterogeneity. *Brain* 2008;**131**:1057–68.
17. Estrada-Sánchez AM, Burroughs CL, Cavaliere S. *et al.* Cortical efferents lacking mutant huntingtin improve striatal neuronal activity and behavior in a conditional mouse model of Huntington's disease. *J Neurosci* 2015;**35**:4440–51.

18. Virlogeux A, Moutaux E, Christaller W. *et al.* Reconstituting corticostriatal network on-a-chip reveals the contribution of the presynaptic compartment to Huntington's disease. *Cell Rep* 2018;**22**:110–22.
19. Gu X, Li C, Wei W. *et al.* Pathological cell-cell interactions elicited by a neuropathogenic form of mutant huntingtin contribute to cortical pathogenesis in HD mice. *Neuron* 2005;**46**: 433–44.
20. Carcea I, Froemke RC. Chapter 3—cortical plasticity, excitatory-inhibitory balance, and sensory perception. In: Merzenich M.M., Nahum M., Van Vleet T.M. (eds.), *Progress in Brain Research*, Vol. **207**. Elsevier, Amsterdam, 2013, 65–90.
21. Sepers MD, Mackay JP, Koch E. *et al.* Altered cortical processing of sensory input in Huntington disease mouse models. *Neurobiol Dis* 2022;**169**:105740.
22. Mazarakis NK, Cybulska-Klosowicz A, Grote H. *et al.* Deficits in experience-dependent cortical plasticity and sensory-discrimination learning in presymptomatic Huntington's disease mice. *J Neurosci* 2005;**25**:3059–66.
23. Cummings DM, André VM, Uzgil BO. *et al.* Alterations in cortical excitation and inhibition in genetic mouse models of Huntington's disease. *J Neurosci* 2009;**29**:10371–86.
24. Indersmitten T, Tran CH, Cepeda C. *et al.* Altered excitatory and inhibitory inputs to striatal medium-sized spiny neurons and cortical pyramidal neurons in the Q175 mouse model of Huntington's disease. *J Neurophysiol* 2015;**113**:2953–66.
25. Spampanato J, Gu X, Yang XW. *et al.* Progressive synaptic pathology of motor cortical neurons in a BAC transgenic mouse model of Huntington's disease. *Neuroscience* 2008;**157**:606–20.
26. Menalled LB, Kudwa AE, Miller S. *et al.* Comprehensive behavioral and molecular characterization of a new knock-in mouse model of Huntington's disease: zQ175. *PLoS One* 2012;**7**:e49838.
27. Heikkinen T, Lehtimäki K, Vartiainen N. *et al.* Characterization of neurophysiological and behavioral changes, MRI brain volumetry and 1H MRS in zQ175 knock-in mouse model of Huntington's disease. *PLoS One* 2012;**7**:e50717.
28. Deng Y, Wang H, Joni M. *et al.* Progression of basal ganglia pathology in heterozygous Q175 knock-in Huntington's disease mice. *J Comp Neurol* 2021;**529**:1327–71.
29. Vormstein-Schneider D, Lin JD, Pelkey KA. *et al.* Viral manipulation of functionally distinct interneurons in mice, non-human primates and humans. *Nat Neurosci* 2020;**23**:1629–36.
30. Philpott AL, Cummins TDR, Bailey NW. *et al.* Cortical inhibitory deficits in premanifest and early Huntington's disease. *Behav Brain Res* 2016;**296**:311–7.
31. Schippling S, Schneider SA, Bhatia KP. *et al.* Abnormal motor cortex excitability in preclinical and very early Huntington's disease. *Biol Psychiatry* 2009;**65**:959–65.
32. Wang Y, Sepers MD, Xiao D. *et al.* Water-reaching platform for longitudinal assessment of cortical activity and fine motor coordination defects in a Huntington disease mouse model. *eNeuro* 2023;**10**:ENEURO.0452–22.2022.
33. Smith GA, Rocha EM, McLean JR. *et al.* Progressive axonal transport and synaptic protein changes correlate with behavioral and neuropathological abnormalities in the heterozygous Q175 KI mouse model of Huntington's disease. *Hum Mol Genet* 2014;**23**: 4510–27.
34. Peng Q, Wu B, Jiang M. *et al.* Characterization of behavioral, neuropathological, brain metabolic and key molecular changes in zQ175 knock-in mouse model of Huntington's disease. *PLoS One* 2016;**11**:e0148839.
35. Southwell AL, Smith-Dijak A, Kay C. *et al.* An enhanced Q175 knock-in mouse model of Huntington disease with higher mutant huntingtin levels and accelerated disease phenotypes. *Hum Mol Genet* 2016;**25**:3654–75.
36. Cummings DM, Milnerwood AJ, Dallérac GM. *et al.* Aberrant cortical synaptic plasticity and dopaminergic dysfunction in a mouse model of Huntington's disease. *Hum Mol Genet* 2006;**15**: 2856–68.
37. Donzis EJ, Estrada-Sánchez AM, Indersmitten T. *et al.* Cortical network dynamics is altered in mouse models of Huntington's disease. *Cereb Cortex* 2020;**30**:2372–88.
38. Johnson EB, Ziegler G, Penny W. *et al.* Dynamics of cortical degeneration over a decade in Huntington's disease. *Biol Psychiatry* 2021;**89**:807–16.
39. Estrada-Sánchez AM, Castro D, Portillo-Ortiz K. *et al.* Complete but not partial inhibition of glutamate transporters exacerbates cortical excitability in the R6/2 mouse model of Huntington's disease. *CNS Neurosci Ther* 2019;**25**:509–18.
40. Mahfooz K, Marco S, Martínez-Turrillas R. *et al.* GluN3A promotes NMDA spiking by enhancing synaptic transmission in Huntington's disease models. *Neurobiol Dis* 2016;**93**:47–56.
41. Khakh BS, Beaumont V, Cachope R. *et al.* Unravelling and exploiting astrocyte dysfunction in Huntington's disease. *Trends Neurosci* 2017;**40**:422–37.
42. Hardingham GE, Bading H. Synaptic versus extrasynaptic NMDA receptor signalling: implications for neurodegenerative disorders. *Nat Rev Neurosci* 2010;**11**:682–96.
43. Xue M, Atallah BV, Scanziani M. Equalizing excitation-inhibition ratios across visual cortical neurons. *Nature* 2014;**511**:596–600.
44. Dougherty SE, Hollimon JJ, McMeekin LJ. *et al.* Hyperactivity and cortical disinhibition in mice with restricted expression of mutant huntingtin to parvalbumin-positive cells. *Neurobiol Dis* 2014;**62**:160–71.
45. Kim EH, Thu DCV, Tippett LJ. *et al.* Cortical interneuron loss and symptom heterogeneity in Huntington disease. *Ann Neurol* 2014;**75**:717–27.
46. Tremblay R, Lee S, Rudy B. GABAergic interneurons in the neocortex: from cellular properties to circuits. *Neuron* 2016;**91**: 260–92.